Title

Promoter–Poison Partnership Protects Platinum Performance in Coked Cluster Catalysts

Authors

Poths, Patricia
Morgan, Harry WT
Li, Guangjing
et al.

Peer reviewed

Promoter-poison partnership protects platinum performance in coked cluster catalysts

Patricia Poths,[*,†] Harry W. T. Morgan,[†] Guangjing Li,[‡] Autumn Fuchs,[‡] Scott L. Anderson,[*,‡] and Anastassia N. Alexandrova[*,†,¶]

†Department of Chemistry and Biochemistry, University of California, Los Angeles, Los Angeles, CA 90095, USA

‡Department of Chemistry, University of Utah, Salt Lake City, UT, 84112, USA

¶California NanoSystems Institute, Los Angeles, CA, 90095, USA

E-mail: patriciapoths@chem.ucla.edu; anderson@utah.edu; ana@chem.ucla.edu

Abstract

Deactivation via coking due to a lack of selectivity is a persistent problem for the longevity of Pt-based dehydrogenation catalysts. Ge as a promoter improves the experimental selectivity and stability of subnano Pt_4 clusters. The origin of this improvement is self-limiting coking, to form a Pt_4GeC_2 cluster which is more stable and selective than the bare Pt_4Ge cluster. In this paper we compare the dehydrogenation abilities of Pt_4 and Pt_4C_2 with and Pt_4Ge and Pt_4GeC_2 with DFT calculations in order to explore the origin of self-limiting coking in the presence of Ge. The unique stability of Pt_4GeC_2 is attributed to electron donation from Ge to the C_2 atoms. This prevents the coke from drawing electrons from the Pt, which is the origin of deactivation via coking, and weakens ethylene binding. Thus, we identify an electronic mechanism for coke deactivation and then use an electronically driven doping strategy to improve catalyst longevity. This differs from the common perception of coke deactivating via steric blocking of active sites. Furthermore, Pt_4C_2 and Pt_4GeC_2 show differences in kinetic accessibility of different isomers, which brings us into a new paradigm of sub-ensembles of isomers, where the dominant active sites are determined by kinetic stability under reaction conditions, rather than Boltzmann populations.

Introduction

The formation of coke, or carbonaceous deposits, is a persistent problem for dehydrogenation catalysts, as it results in their rapid deactivation. Deactivation is typically attributed to physical blocking of active sites on the catalyst. Coke formation on Pt-based alkane dehydrogenation catalysts originates from the lack of selectivity of the catalyst; side reactions for deeper dehydrogenation past alkenes and C-C cleavage contribute to coke formation. Approaches to preventing coke formation include co-feeding H_2,[1] changing Pt nanoparticle size,[2] and dopants or promoters such as Sn,[3–5] Ge,[6,7] Si,[8] Ga,[9–11] Zn,[12] and B.[13–15] These approaches all favor desorption of the desired alkenes over deeper dehydrogenation or side-

reactions.

Coke formation typically occurs in two stages; an initial fast coking regime, and a later regime where the buildup of further coke is much slower,[16,17] which indicates that early coking stages change catalysts selectivity to limit further coking. This change in selectivity has been attributed to carbon blocking the most reactive and least selective sites, which can catalyze side-reactions leading to coke formation.[18–23] An additional explanation is that the presence of carbon can modify olefin adsorption strength on a surface, and increase the energy barrier for C-H activation.[17] Coke may therefore deactivate Pt catalysts via an electronic interaction, in addition to steric blocking.

The interaction between metal and coke influencing selectivity is reminiscent of dopants or promoters; the selectivity improvement from adding Sn or Ge to the Pt catalyst comes at the cost of activity, though not to the same extent as coking. Sn is the most widely-used dopant for Pt, though Ge has been found to produce similar improvements in stability against coking.[20–23] XPS of subnano PtSn clusters shows a shift to lower binding energies, implying that Sn tends to donate electrons to Pt.[3] However, there have been reports that PtSn catalysts build up more coke than their pure Pt analogues,[24] suggesting that they are not simply resistant to the build-up of coke, but that their activity persists despite partial coking. The contrast between the electronic and steric mechanisms of coking, and the role of doping are represented in Figure 1.

Sub-nano clusters are promising catalysts due to their high atom utility, and ability to outperform bulk-like catalysts by breaking scaling relations.[25] Pure Pt clusters have been studied as alkane dehydrogenation catalysts,[26] as have various dopants to improve catalyst selectivity, including B,[14] Si,[8] Ge[7] Sn,[3–5] and S.[27] Previous computational and experimental work investigating the role of dopants has spanned a number of supports; PtSn clusters have been explored on both SiO_2 and Al_2O_3,[3–5] showing similar effects of doping on selectivity and stability, regardless of support. Additionally, PtB clusters have been investigated on MgO[13]
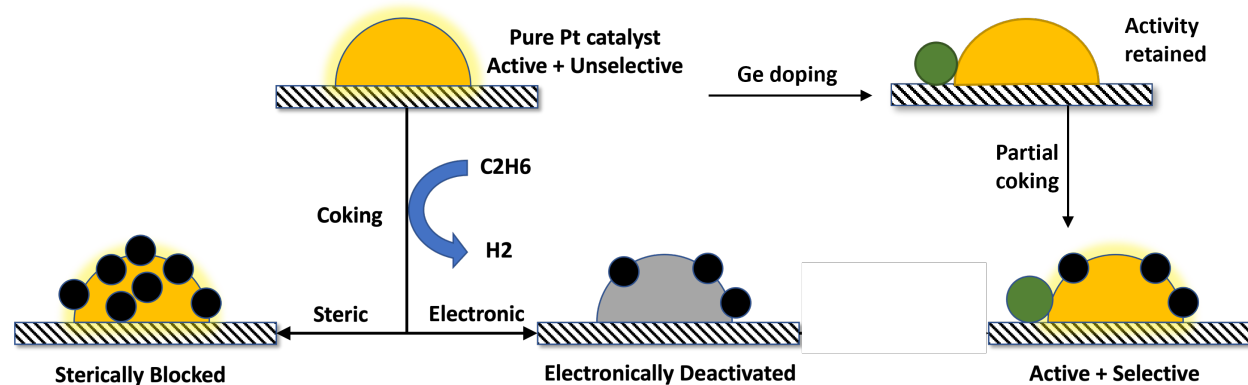
Figure 1: Schematic showing the steric and electronic deactivation mechanisms of coked platinum catalysts, and the activity-preserving effect of doping on partially coked catalysts.

and Al_2O_3,[14] also showing similar effects of the dopant independent of the support. The prediction of Ge as a superior dopant via DFT was based on MgO as the support, which was substantiated by experiment on Al_2O_3, also showing that the role of dopant can be generalized across support.[7,28] Surface-supported clusters are fluxional, isomerizing rapidly under the high temperatures of real reactions such that metastable structures are thermally populated.[29] Higher-energy isomers often show greater catalytic activity than the global minimum isomer.[28,30,31] If the kinetic barriers for isomerisation are low, then the isomer populations will be determined by a Boltzmann distribution.[32] If a cluster were to have high isomerisation barriers then the ensemble would not thermally equilibrate, and macroscopic properties would be determined by the reduced set of accessible isomers, which could be useful if the prevalent isomers have superior activity.[33]

We recently predicted and observed that Ge-doped Pt_4 subnanoclusters, supported on Al_2O_3, display superior stability over pure Pt_4 due to the formation of a carbon-containing species Pt_4GeC_2, which is resistant to deactivation by coke and is predicted to be a catalyst for ethane dehydrogenation.[7,28] This parallels the behavior of PtSn nanoparticles which remain active despite building up more coke than their pure Pt analogues.[24] Transforming a poisoning process into in-situ catalyst synthesis by doping, illustrated in the right-most part of Figure 1, is a key aspect of catalyst design that deserves greater attention. To apply this

strategy to other reactions, we must first understand the fundamental chemistry behind the efficacy of Pt_4GeC_2.

In this paper we investigate the electronic synergy between Ge and coke in Pt_4 clusters in the context of ethane dehydrogenation with a combination of DFT calculations and experiment. For the DFT calculations, we focus on the "pristine" clusters Pt_4 and Pt_4Ge, and their partially coked counterparts Pt_4C_2, and Pt_4GeC_2. After obtaining the ensemble of isomers, we perform transition state calculations to obtain barriers and determine the reactivities of these isomers towards ethane and ethylene dehydrogenation. Bonding analysis of the interaction between Ge and C_2 provides a chemical explanation of the stability trends. With supporting experimental evidence from ISS and TPD data, we observe that Ge mitigates the deactivating effect of C towards ethane dehydrogenation, and improves the selectivity towards ethylene desorption. In order to best match the previous experimental results,[28] which are performed under UHV surface science conditions, we have performed the DFT calculations without additional coverage of H_2, which additionally best matches conditions for the endothermic cooling of supersonic jets, a potential application for ultra-selective direct dehydrogenation catalysts in the absence of any added H_2. While H_2 is added to the chemical feed in industrial ethane dehydrogenation to improve selectivity, here we explore changes in selectivity independent of this factor, and presume conditions where added H_2 would not be present.

Methods

Computational Methods

Calculations on surface-supported clusters were performed using plane-wave DFT in VASP,[34] using the PBE exchange-correlation functional,[35] PAW pseudopotentials,[36] DFT-D3 dispersion correction,[37] and a plane-wave cut-off of 500 eV. Unit cells were constructed from a 5-layer 3x3 supercell of α-Al_2O_3 with a 15 Å vacuum gap, which was previously optimized.[26]

Transition states were calculated using the climbing-image nudged elastic band (CI-NEB) method implemented in VTST.[38,39] Due to the large number of barriers calculated in the study, we have not performed frequency calculations for each TS. QTAIM analysis was performed using the Bader code developed by the Henkelman group.[40,41]

Global optimizations were performed with a BLDA approach[42] to generating chemically-reasonable initial structures, both for cluster structure sampling, and adsorbate binding sampling. For the adsorbate binding, we explored C-H activation without additional coverage of H_2, in order to best match the surface science conditions of the experiment, where D_2 is observed to readily desorb from the clusters during TPD cycles.[28] The in-house codes PGOPT and GOCIA were used to run the global optimizations.

Local-basis projections for bonding analysis were performed with LOBSTER,[43] using the PBEVaspFit basis set and a projection basis of $5p5d6s$ for Pt, $4s4p$ for Ge, $3s3p$ for Al, and $2s2p$ for C and O.[44,45] All projections reported less than 1.2% charge spilling.

DFT calculations on gas-phase models were performed with the Amsterdam Density Functional (ADF) package,[46] version 2019.304, using the PBE functional.[35] Slater-type basis sets of triple-ζ + polarization quality were used on all atoms, with orbitals up to 4d (Pt), 3d (Ge) and 1s (C) included in the frozen core.[47]

Experimental Methods

The relative intensities in He$^+$ ion scattering spectroscopy (ISS) was summarized from the series of ISS previous results for Pt_4/alumina and Pt_4Ge/alumina.[28] The relative intensities are calculated by taking the average Pt ISS signals of the first 3 data points of the corresponding series of ISS, of which the ISS signals are calculated by integrating the background subtracted Pt integrated intensities normalized to the total integrated ISS signals for the full ion scattering spectrum that remain relatively invariant to compensate for the fluctuation of He$^+$ ions scattered. The Pt ISS signals for the as deposited samples are extrapolated, to reveal what the initial Pt ISS signals would be at, from the gradual leveled curve rising from

the ISS intensities after some exposure of the samples under He + ions; the extrapolated numbers are close to their corresponding Pt ISS signals post 750 K heat treatment, thus indicating the presence of adventitious adsorbates or H and Cl atoms present on the sample surfaces as well as that the clusters do not sinter much after a single heat treatment on the sample surface.

The C_2D_4 adsorbed molecules per cluster are calculated from the sum of the high temperature C_2D_4 desorption peaks (attributed to C_2D_4 binding to Pt) and half of the D_2 desorbed molecules (as each C_2D_4 produces 2 D_2 molecules) in the temperature programmed desorption from our previous work.[28]

Results and discussion

Cluster Ensembles

In order to understand why Pt_4GeC_2 is a stable and selective catalyst, while Pt_4 continues to coke, we compute the geometries and C-H activation barriers of ethane, ethylene, and acetylene on Pt_4 and Pt_4C_2, and compare them to equivalent results for Pt_4Ge and Pt_4GeC_2.[28] The compositions Pt_4 and Pt_4Ge were chosen, as described in our previous work,[28] based on experimental compositions determined via XPS.

Figure 2 shows the full ensembles for Al_2O_3-supported (a) Pt_4, (b) Pt_4C_2, (c) Pt_4Ge, and (d) Pt_4GeC_2. Atomic Bader charges are shown on or near their corresponding atoms. Most Pt motifs are common to Pt_4 and Pt_4Ge, with Ge sitting on the edge of the Pt core. Addition of C_2 induces dramatic restructuring of both clusters, but the isomers for Pt_4C_2 and Pt_4GeC_2 are nonetheless very similar. Note the similarity between the Pt_4C_2 and Pt_4GeC_2 global minimum (GM) structures, as well as the similarity between the structures with the intact C_2 unit incorporated into the center of the cluster. The C atoms are mostly 3-coordinate and there are two motifs of carbon binding; either the C_2 unit has been split, or it remains intact. The Pt atoms are on the edges of the clusters, so incorporation of C into the Pt_4
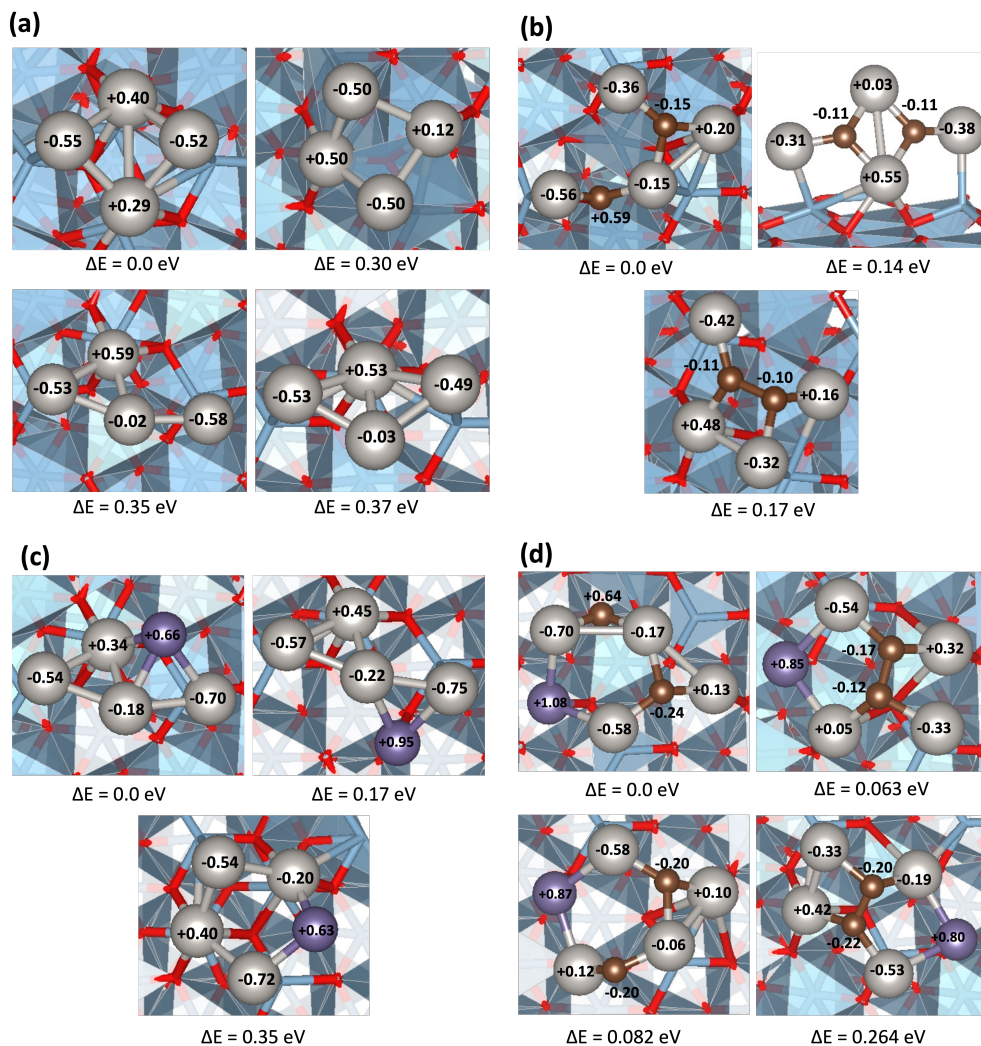
7

Figure 2: Thermally accessible structures obtained via global optimization for alumina-supported (a) Pt_4, (b) Pt_4C_2, (c) Pt_4Ge, and (d) Pt_4GeC_2. Bader charges are shown on or near each corresponding atom. Side views shown in Figure S1.

cluster does not block Pt sites from interacting with gas-phase molecules. This contrasts with the conventional view of coke poisoning, which is that the Pt core retains its initial structure and active sites are blocked by a layer of carbon. Pt sites in these structures are still exposed after coking, which suggests that coke alters the activity and selectivity of Pt subnanoclusters through electronic effects, rather than by steric blocking. This agrees with literature which suggests an electronic component to deactivation via coke formation.[16,17] Thus, the particular stability of Pt_4GeC_2 must arise from a combination of electronic effects

that work together to enhance selectivity without sacrificing activity.

The computed Bader charges are our first piece of evidence for the nature of these electronic effects. Ge always has a strong positive charge, as expected from relative electronegativities of Pt vs. Ge. In contrast, C atoms are negatively charged, which increases in magnitude in the presence of Ge. The average charge on Pt becomes increasingly negative upon addition of Ge, and becomes increasingly positive upon addition of C_2. However, the charges on individual Pt atoms depends strongly on the location of Pt relative to the Al_2O_3 surface. The structure of the Pt_4 clusters in Figure 2a is such that the Pt atoms closer to the support bind primarily to multiple oxygens of the surface, adopting a positive charge. Pt atoms in the upper layer of the cluster are generally located over Al atoms, adopting a negative charge while distorting the surface by pulling Al up. Pt atoms that are not directly bound to the surface tend to adopt a very slight negative charge, but are almost charge neutral. The inclusion of C, while generally decreasing the electron density on the Pt clusters, mainly results in a more positive (or less negative) charge on the Pt atoms directly bound to it, regardless of which surface atoms they are additionally bound to. Ge, similarly, results in a more negative (or less positive) charge on the Pt atoms directly bound to it, again regardless of the surface atoms also bound to Pt. The combination of Ge and C_2 bound to the cluster essentially pushes electrons from Ge to C, via Pt, ultimately resulting in a more negative charge on Pt atoms via synergistic electronic effects.

So far we have described the isomeric ensembles of the 'bare' clusters, without adsorbates. Once we bind ethane, ethylene, and acetylene, the relative stabilities of the different Pt_4C_2 and Pt_4GeC_2 core structures change. For Pt_4C_2, binding ethylene and acetylene favors the isomer with the intact C_2 unit, to the point where the C_2H_2/Pt_4C_2 ensemble only contains Pt_4C_2 core structures with the intact C_2, and the C_2H_4/Pt_4C_2 ensemble only has the split isomer at higher energies (Fig S2). For Pt_4GeC_2 the distinction between C-C bonded and split isomers is especially important because the latter do not contribute to catalysis. Binding energy calculations suggest that ethane will physisorb to the split isomer (Fig. S4), but

9

as there is no chemical bond between the ethane and the cluster, we can consider this isomer to be inactive. The C-C bonded isomer, which lies just 0.06 eV above the global minimum isomer in the absence of adsorbates, has ethane C-H activation barriers ranging from 0.42-0.50 eV, and so is catalytic.[28] Furthermore, once ethylene and acetylene bind to Pt_4GeC_2, the bonded isomer dominates the ensembles and the split isomer is pushed much higher in energy (Fig. S4). For Pt_4C_2, the split isomer, while less reactive towards ethane (barriers ranging between 0.6-0.9 eV), is more reactive towards ethylene, with a C-H activation barrier 0f 0.80 eV (Fig S3). The accessible binding modes for ethane and ethylene on Pt_4C_2 show a wider range of cluster cores than for Pt_4GeC_2 (as mentioned above, see SI for the structures), each of which with variable reactivity. We attribute this difference in activity of the split isomer in Pt_4C_2 compared to Pt_4GeC_2 to the fact that the Pt centers that bind ethane and ethylene in the split Pt_4C_2 isomer are bonded to Ge in Pt_4GeC_2 and therefore have very different electronic character. The relationship between isomerism and reactivity in Pt_4GeC_2 makes it important for us to establish the relative populations of the split and bonded isomers. The barrier to direct interconversion is 1.33eV (Fig. S5), placing Pt_4GeC_2 in the unusual non-Boltzmann regime where the isomers do not thermally equilibrate. The populations will instead be determined by their formation rates, which are equivalent to the relative rates of dehydrogenation and C-C cleavage on Pt_4Ge. We will discuss the kinetic data for these processes later.

Activity vs. Selectivity

To explore the balance of activity and selectivity of Pt_4, Pt_4C_2, Pt_4Ge, and Pt_4GeC_2, we plot the C-H activation barriers against the adsorption energies for ethane and ethylene, as shown in Figure 3 (a) and (b), respectively. The balance between adsorption energy and activation energy is a useful descriptor of reactivity because it captures the two main competing processes for an adsorbate bound to a catalyst. Each point represents an isomer and binding mode, so this representation accounts for the effect of cluster fluxionality. The cor-

responding ethane and ethylene isomer ensembles and C-H activation barriers can be found in the SI. The colored shapes reflect the isomer distributions of each cluster composition, and are intended only to highlight general trends in composition and catalytic properties. The dashed line represents where the (first) C-H activation barrier is equal in magnitude to the adsorption energy. Note that we use the first C-H activation barrier as the rate limiting step, as has been previously shown,[48] however to validate this, we calculated the second C-H activation barriers for ethane on the Pt_4, Pt_4C_2, Pt_4Ge, and Pt_4GeC_2 isomers with the lowest first C-H activation barriers. All the second C-H barriers are lower than the first one (Fig. S6). The lower-left region of each graph in Figure 3 describes strong binding and low C-H activation barriers, which favors dehydrogenation, while the upper-right region describes weak binding and high barriers, which favors desorption. An optimal selective catalyst will
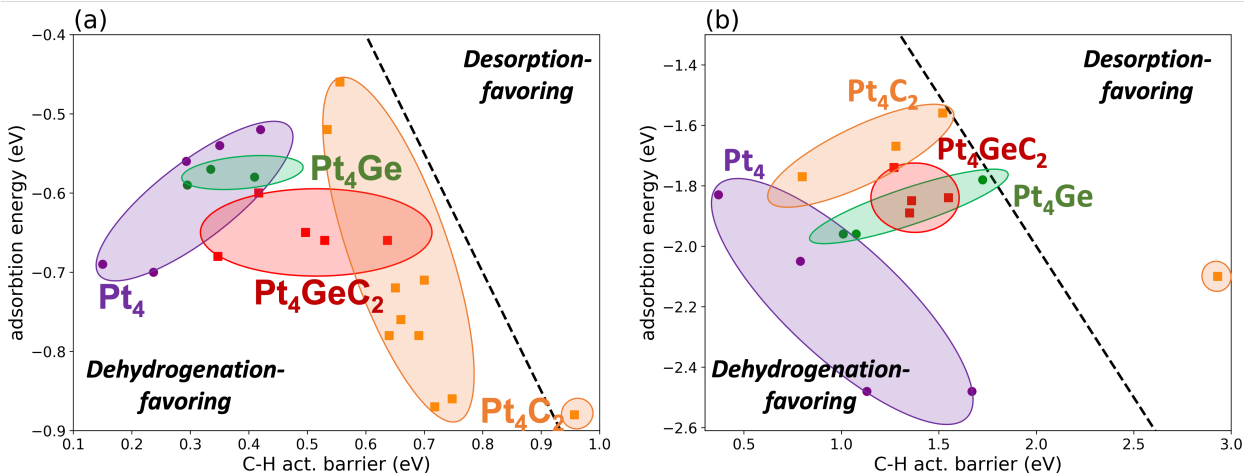

Figure 3: Comparison between adsorption energy and first C-H activation barrier per given isomer of Pt_4, Pt_4C_2, Pt_4Ge, and Pt_4GeC_2 for (a) ethane and (b) ethylene. The dashed line represents where the adsorption energy is equal to that of the C-H activation barrier. The closer the given points are to the upper right corner, the more desorption-favoring that given adsorbate binding mode is; the closer to the bottom left, the more dehydrogenation-favoring the binding mode.

appear in the lower-left region of the ethane graph, as ethane dehydrogenation is the target reaction, and the upper-right region of the ethylene graph, as this is our desired product and dehydrogenation of ethylene will lead to coking. The adsorption energies are not corrected for the entropy of the adsorbate in the gas phase, to improve comparability between the

adsorption and activation energies. This entropy correction is the same for all clusters on a graph, so it does not affect our conclusions about the effects of coking or doping on activity and selectivity. Furthermore, the precise entropy of ethylene in the gas phase depends on the conversion of ethane to ethylene, which we cannot determine in a straightforward way from these calculations.

For ethane (Fig. 3(a)), we see that Pt_4 is the most active composition, as its points are furthest away from the dashed line, i.e. the C-H activation barrier is lowest compared to the adsorption energy of ethane. Pt_4Ge overlaps with the Pt_4 distribution, indicating that the two have similar activities. Compared to Pt_4, Pt_4C_2 has a much wider spread of points that are closer to the dashed line, showing that small coke deposits deactivate Pt for ethane dehydrogenation. Pt_4GeC_2 on the other hand does not shift so dramatically compared to Pt_4Ge, with adsorption energies and C-H activation barriers both increasing slightly when carbon is added. The Pt_4GeC_2 points remain clustered quite close to Pt_4 and Pt_4Ge, indicating that a small amount of coke does not significantly deactivate Pt_4Ge for ethane dehydrogenation. For activity towards ethylene (Fig. 3(b)), we see a different trend with composition. The Pt_4 points are much farther from the dashed line than all other cluster compositions, highlighting the tendency for Pt_4 to dehydrogenate ethylene and coke. All other cluster compositions, with dopant and/or poison, are located much closer to the dashed line, indicating increased preference for desorption of ethylene over dehydrogenation. The GM $C_2H_{4/}Pt_4C_2$ isomer is an outlier, binding ethylene strongly but having a very large activation barrier, while the higher-energy isomers are grouped in a region with weak binding and surmountable barriers. In contrast, the Pt_4Ge and Pt_4GeC_2 regions in Figure 3a are clustered close to the dashed line, indicating superior selectivity for ethylene desorption to Pt_4.

One aspect that Figure 3 does not capture is the tendency for side-reactions, such as cleavage of the C-C bond preferentially over the C-H bond, to compete. This is known to be a coke-promoting side reaction on Pt catalysts,[16–19] and that the addition of dopants limits

12

their occurrence.[12,22,49–51] In order to assess the preference for C-C vs. C-H cleavage of Pt_4, Pt_4C_2, Pt_4Ge, and Pt_4GeC_2, we computed C-C bond breaking barriers for isomers where we already had the barriers for C-H activation. These results are summarized in Table S1 and Figure S7. Ultimately, we find for Pt_4, once acetylene forms, the barrier for C-C bond breaking is lower than that of C-H activation (0.76 eV compared to 0.97 eV). Prior to acetylene formation, however, C-H activation is preferential. This agrees with literature.[16–18] This also holds for Pt_4C_2; only for acetylene does C-C cleavage have a lower barrier than C-H activation. However, in the presence of coke, all barriers are greater, reflecting the general deactivation of the catalyst. Thus, for the Pt_4C_2 ensemble, it is possible to access the split C_2 isomer via splitting of acetylene, prior to dehydrogenation. This enables the full Pt_4C_2 ensemble to be kinetically accessible. In contrast, Pt_4Ge always favors C-H activation over C-C cleavage, regardless of the adsorbate. Not only does this prevent a coke-forming side-reaction, but this also kinetically traps the ensemble into structures with the intact C_2 unit, which, as mentioned above, is in fact the active isomer for ethane activation.

Bonding Analysis

The next question is, 'How do Ge and C_2 interact to produce a coke-resistant cluster cata-lyst?'. To answer this question we calculate integrated crystal orbital Hamilton populations (ICOHPs)[44] for C-C bonds in Pt_4C_2 and Pt_4GeC_2, and the species formed when each of these binds an ethylene molecule, C_2H_4/Pt_4C_2 and C_2H_4/Pt_4GeC_2. This analysis is done for isomers which contain carbon in the form of C-C dimers, rather than separated C atoms, due to their greater activity and accessibility as Pt_4GeC_2. These isomers are the most catalyti-cally important (Figs S3, S4), and the structural similarities between the doped and undoped clusters allow us to draw conclusions about the electronic effects of doping. The results are shown in Figure 4, where the ICOHPs are shown (blue annotations) alongside the respective C-C bonds. Comparing Pt_4C_2 to Pt_4GeC_2 we find that doping with Ge increases the C-C ICOHP from -11.5 eV to -12.8 eV; added Ge enhances the C-C bond strength. Molecular
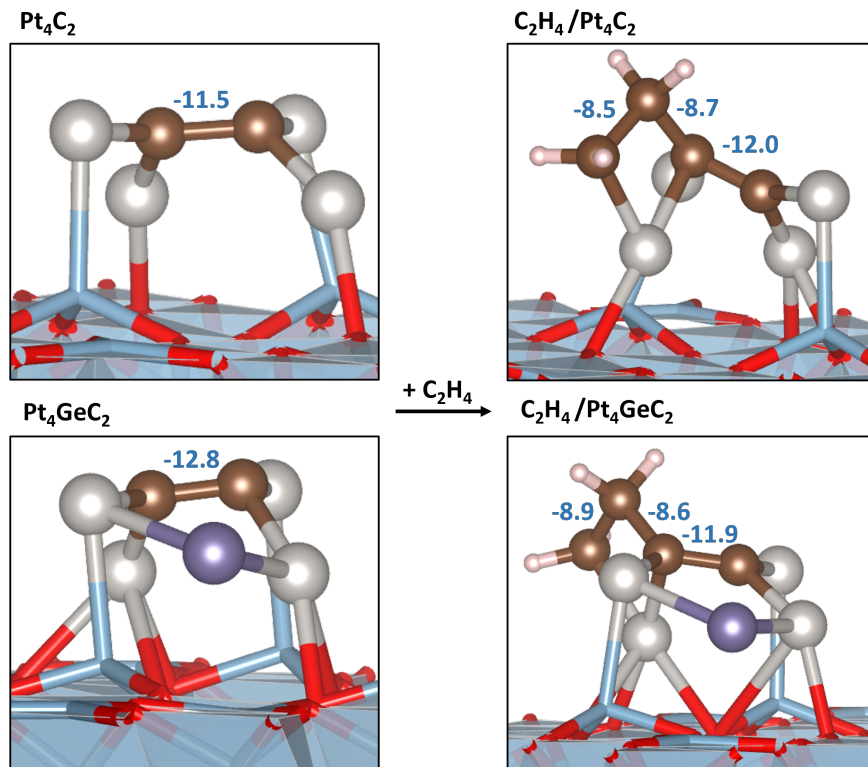
13

Figure 4: C-C ICOHPs (blue numbers, units of eV) for Pt_4C_2 (upper left), Pt_4GeC_2 (lower left), C_2H_4/Pt_4C_2 (upper right), and C_2H_4/Pt_4GeC_2 (lower right).

orbitals (Fig. S8), density of states, and COHPs (Fig. S9) show that this is due to Ge donating electrons into a C-C π-bonding orbital. The bond strength comparison explains energetic differences in the isomer distributions of Pt_4C_2 and Pt_4GeC_2 in Figure 2 - in Pt_4C_2 the isomer with the C-C bond is 0.17 eV above the global minimum, in which the C atoms are separated, while the energy gap between equivalent isomers of Pt_4GeC_2 is only 0.06 eV. Next, we compare Pt_4C_2 and Pt_4GeC_2 isomers with ethylene bound to both Pt and to the C_2 unit. When binding a C_2H_4 molecule, the intra-cluster C-C bond in Pt_4C_2 is strengthened (ICOHP rises from -11.5 eV to -12.0 eV), while the equivalent bond in Pt_4GeC_2 is weakened (ICOHP falls from -12.8 eV to -11.9 eV). This implies that Ge weakens the binding of ethylene to Pt_4GeC_2 because the internal C-C bond must be partially broken, while the initially weaker bond in Pt_4C_2 is strengthened by binding ethylene. Pt_4GeC_2 is therefore resistant to coking relative to Pt_4C_2. This is reflected in the ethylene binding energies, which are -2.10

14

eV for Pt_4C_2 and -1.85 eV for Pt_4GeC_2.

Role of Ge Content in C-C interactions

We have determined that doping with Ge strengthens the C-C bond in Pt_4GeC_2, so we wish to know whether this behavior is general. Since the bond strength maps onto the relative energies of isomers with C atoms bonded or separated, we can screen isomers and categorise them by the numbers of C-C and Pt-C bonds, which is more efficient than bonding analysis with ICOHP. We performed global optimizations of $Pt_4Ge_xC_2$ (x = 0-2) and in Figure 5 we plot the numbers of C-C (orange) and Pt-C (blue) bonds in each isomer vs isomer energy. The orange points show the number of C-C bonds, defined as a C-C distance of less than
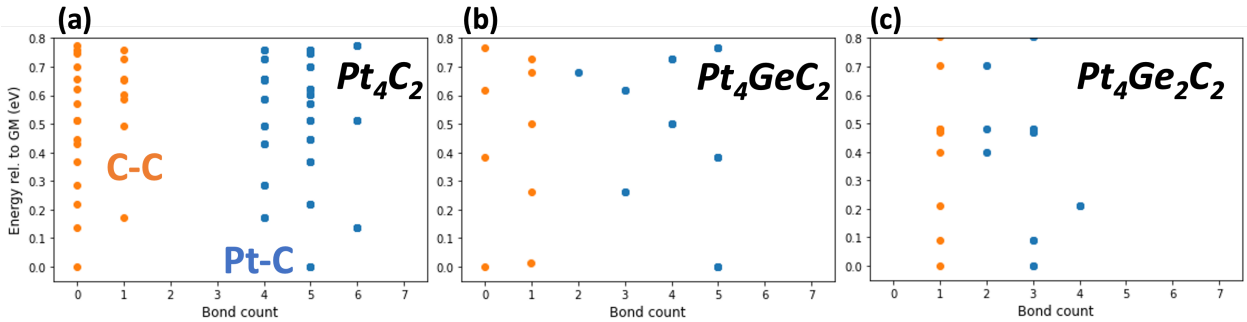

Figure 5: Plots showing number of C-C and Pt-C bonds agains the energy of a given isomer relative to the GM structure for (a) Pt_4C_2, (b) Pt_4GeC_2, and (c) $Pt_4Ge_2C_2$, showing the dependence of number of C-C bonds with Ge content for $Pt_4Ge_xC_2$ clusters.

1.75 Å, which can only be 0 or 1 here. In Pt_4C_2 most of the low-energy isomers have no C-C bond, while Pt_4GeC_2 shows a more even distribution of C-C separated and bonded isomers, and $Pt_4Ge_2C_2$ features only C-C bonded isomers. The blue points show the number of Pt-C bonds in each isomer, defined by a 2.25 Å cutoff length. The number of Pt-C bonds falls as the amount of Ge in the cluster increases, from 4-6 in Pt_4C_2 to 2-4 in $Pt_4Ge_2C_2$. It therefore appears that strengthening C-C bonds by Ge doping causes clusters to adopt structures with more C-C bonds at the expense of Pt-C bonds. The phenomenon of Ge doping strengthening C-C bonding appears to be general across a range of Ge concentrations, and we anticipate that this could be extended to other Pt_n cluster sizes.

15

Experimental Support

We previously reported a study of desorption, decomposition, and carbon deposition on Pt_4 and Pt_4Ge supported on alumina thin films, measured by temperature programmed desorption (TPD) experiments.[28] For the readers convenience, the experimental methodology is briefly summarized in the SI. The Pt ISS intensities and the numbers of C_2D_4 molecules adsorbed during the low temperature C_2D_4 dose prior to TPD runs are quantified in Figure 6 in a way that facilitates comparison to the DFT results presented here. Results are given for
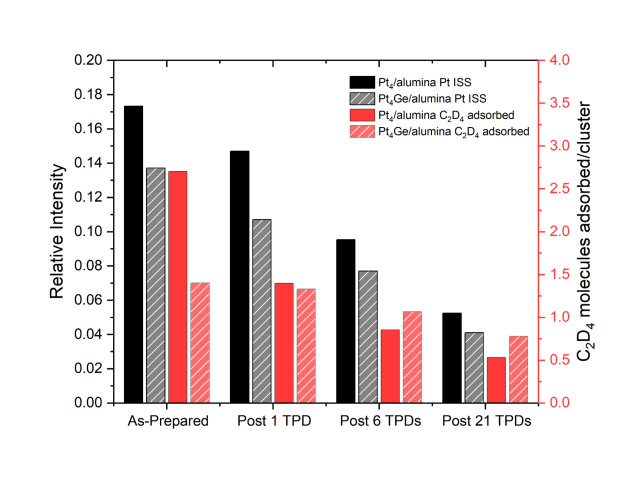

Figure 6: Pt relative intensities from He^+ ion scattering spectroscopy of Pt_4/alumina (black) and Pt_4Ge/alumina (hatched grey). The secondary axis highlights the number of C_2D_4 molecules adsorbed to Pt sites on Pt_4/alumina (red) and Pt_4Ge/alumina (hatched light red) per cluster.

as-prepared Pt_4/alumina and Pt_4Ge/alumina, i.e., ISS intensities measured for as-prepared samples, and C_2D_4 molecules adsorbed extracted from analysis of the first TPD runs on fresh, separately prepared samples. Results are also summarized for the Pt ISS intensities and C_2D_4 molecules adsorbing for samples prepared and then subjected to 1 TPD run, 6 TPD runs, and 21 TPD runs, all obtained with separately prepared samples to avoid sample damage from ISS. The numbers of C_2D_4 molecules adsorbed on the samples are indicative of the number of ethylene binding sites available at different stages of reaction/deactivation, and the Pt ISS intensities are proportional to the fraction of the deposited Pt atoms (identical in all samples) that are He^+ accessible in the topmost sample layer. Both the numbers of

C_2D_4 molecules adsorbing, and the fraction of exposed Pt atoms are adversely affected by the carbon deposition and/or Pt sintering that occurs during ethylene TPD, particular for the Pt_4/alumina samples. It is clear, however, that TPD has quite different effects on the two measurements. We see that, while both the number of Pt sites and the number of C_2D_4 molecules desorbing attenuate, they do not attenuate to the same extent for either Pt_4 or Pt_4Ge. Pt sites remain even when the total number of C_2D_4 sites, measured by number of molecules adsorbed, have decreased. This suggests both that the deactivation via coke formation is electronic in nature, rather than physical blocking of sites, and that coke induces restructuring of the Pt clusters, where Pt sites remain accessible. For Pt_4Ge, we see that the overall attenuation is less for both Pt sites, and C_2D_4 molecules adsorbed, and that the number of molecules adsorbed decreases less relative to attenuation of Pt sites compared to Pt_4.

Conclusions

We have studied the electronic behavior of four dehydrogenation catalysts, Pt_4, Pt_4C_2, Pt_4Ge, and Pt_4GeC_2, all supported on α-Al_2O_3, to explore the role that Ge plays in mitigating deactivation via coke formation. Pt_4 is predicted to be a potent ethane dehydrogenation catalyst, but suffers from poor selectivity, driving deep dehydrogenation that leads to carbon deposition and catalyst deactivation. This deactivation is attributed to electronic effects, as coke formation does not primarily block sites, but changes the electronic properties of the cluster, with the C_2 unit withdrawing electron density from Pt while triggering restructuring. Comparison between calculated adsorption energies and C-H activation barriers show that Pt_4Ge is more selective than Pt_4, and the partially coked Pt_4GeC_2 is even more selective. In Pt_4GeC_2, Ge donates electrons to C, preventing the depletion of electron density on Pt, allowing it to retain activity despite some coke formation. Additionally, Ge strengthens the C-C bond in Pt_4GeC_2 and disfavors further binding of coke to the C_2 unit. Thus, Pt_4GeC_2 is

an active dehydrogenation catalyst despite carbon deposition, with desirable selectivity arising from the interaction between Ge and C_2. In contrast, we see that while Pt_4C_2 becomes technically more selective than Pt_4, this comes at the cost of activity, emphasizing that the role of Ge is to help retain activity even when the cluster is lightly coked. Furthermore, by varying Ge content of Pt_4C_2 clusters between 0 and 2, we show that added Ge favors the formation of C-C bonds in the cluster ensembles, favoring structures which tend to retain activity towards ethane. The *ab initio* results are substantiated by experimental results, which demonstrate that the loss of accessible ethylene binding sites during coking is insufficient to explain loss of activity, reflecting that the effect observed for both Pt_4 and Pt_4Ge is electronic rather than steric. The cooperative interaction between Ge and C_2 invites us to see the two species as co-dopants for Pt_4, where Ge as a promoter prevents the poisoning effect of C_2 alone. We believe that the observations reported here help to explain the behavior of other coke-resistant catalysts, and should be applicable to other compositions and reactions.

Acknowledgement

Supporting Information Available

Computed ensembles for Pt_4, Pt_4C_2, Pt_4Ge, and Pt_4GeC_2 both bare and with adsorbed C_2H_6, C_2H_4, and C_2H_2. MO analysis of Pt_4C_2 vs. Pt_4GeC_2. Structures corresponding with C-H activation and C-C bond breaking NEBs. Comparison between C-H and C-C breaking barriers.

References

(1) Sattler, J. J. H. B.; Beale, A. M.; Weckhuysen, B. M. Operando Raman spectroscopy study on the deactivation of Pt/Al2O3 and Pt–Sn/Al2O3 propane dehydrogenation catalysts. *Physical Chemistry Chemical Physics* **2013**, *15*, 12095.

(2) Zhang, W.; Wang, H.; Jiang, J.; Sui, Z.; Zhu, Y.; Chen, D.; Zhou, X. Size Dependence of Pt Catalysts for Propane Dehydrogenation: from Atomically Dispersed to Nanoparticles. *ACS Catalysis* **2020**, *10*, 12932–12942.

(3) Gorey, T. J.; Zandkarimi, B.; Li, G.; Baxter, E. T.; Alexandrova, A. N.; Anderson, S. L. Preparation of Size- and Composition-Controlled Pt $_n$ Sn $_x$ /SiO $_2$ ($n = 4, 7, 24$) Bimetallic Model Catalysts with Atomic Layer Deposition. *The Journal of Physical Chemistry C* **2019**, *123*, 16194–16209.

(4) Zandkarimi, B.; Gorey, T. J.; Li, G.; Munarriz, J.; Anderson, S. L.; Alexandrova, A. N. Alloying with Sn Suppresses Sintering of Size-Selected Subnano Pt Clusters on SiO $_2$ with and without Adsorbates. *Chemistry of Materials* **2020**, *32*, 8595–8605.

(5) Li, G.; Zandkarimi, B.; Cass, A. C.; Gorey, T. J.; Allen, B. J.; Alexandrova, A. N.; Anderson, S. L. Sn-modification of Pt $_7$ /alumina model catalysts: Suppression of carbon deposition and enhanced thermal stability. *The Journal of Chemical Physics* **2020**, *152*, 024702.

(6) Huang, Z.; Fryer, J. R.; Park, C.; Stirling, D.; Webb, G. Transmission Electron Microscopy, Energy Dispersive X-Ray Spectroscopy, and Chemisorption Studies of Pt–Ge/γ-Al2O3Reforming Catalysts. *Journal of Catalysis* **1998**, *175*, 226–235.

(7) Jimenez-Izal, E.; Liu, J.-Y.; Alexandrova, A. N. Germanium as key dopant to boost the catalytic performance of small platinum clusters for alkane dehydrogenation. *Journal of Catalysis* **2019**, *374*, 93–100.

(8) Jimenez-Izal, E.; Zhai, H.; Liu, J.-Y.; Alexandrova, A. N. Nanoalloying MgO-Deposited Pt Clusters with Si To Control the Selectivity of Alkane Dehydrogenation. *ACS Catalysis* **2018**, *8*, 8346–8356.

(9) Sattler, J. J. H. B.; Gonzalez-Jimenez, I. D.; Luo, L.; Stears, B. A.; Malek, A.; Barton, D. G.; Kilos, B. A.; Kaminsky, M. P.; Verhoeven, T. W. G. M.; Koers, E. J. et al. Platinum-Promoted Ga/Al$_2$O$_3$ as Highly Active, Selective, and Stable Catalyst for the Dehydrogenation of Propane. *Angewandte Chemie International Edition* **2014**, *53*, 9251–9256.

(10) Payard, P.-A.; Rochlitz, L.; Searles, K.; Foppa, L.; Leuthold, B.; Safonova, O. V.; Comas-Vives, A.; Copéret, C. Dynamics and Site Isolation: Keys to High Propane Dehydrogenation Performance of Silica-Supported PtGa Nanoparticles. *JACS Au* **2021**, *1*, 1445–1458.

(11) Raman, N.; Wolf, M.; Heller, M.; Heene-Würl, N.; Taccardi, N.; Haumann, M.; Felfer, P.; Wasserscheid, P. GaPt Supported Catalytically Active Liquid Metal Solution Catalysis for Propane Dehydrogenation–Support Influence and Coking Studies. *ACS Catalysis* **2021**, *11*, 13423–13433.

(12) Cybulskis, V. J.; Bukowski, B. C.; Tseng, H.-T.; Gallagher, J. R.; Wu, Z.; Wegener, E.; Kropf, A. J.; Ravel, B.; Ribeiro, F. H.; Greeley, J. et al. Zinc Promotion of Platinum for Catalytic Light Alkane Dehydrogenation: Insights into Geometric and Electronic Effects. *ACS Catalysis* **2017**, *7*, 4173–4181.

(13) Dadras, J.; Jimenez-Izal, E.; Alexandrova, A. N. Alloying Pt Sub-nano-clusters with Boron: Sintering Preventative and Coke Antagonist? *ACS Catalysis* **2015**, *5*, 5719–5727.

(14) Ha, M.-A.; Baxter, E. T.; Cass, A. C.; Anderson, S. L.; Alexandrova, A. N. Boron

Switch for Selectivity of Catalytic Dehydrogenation on Size-Selected Pt Clusters on Al2O3. *J. Am. Chem. Soc.* **2017**, 8.

(15) Aly, M.; Fornero, E. L.; Leon-Garzon, A. R.; Galvita, V. V.; Saeys, M. Effect of Boron Promotion on Coke Formation during Propane Dehydrogenation over Pt/γ-Al2O3 Catalysts. *ACS Catalysis* **2020**, *10*, 5208–5216.

(16) Lian, Z.; Ali, S.; Liu, T.; Si, C.; Li, B.; Su, D. S. Revealing the Janus Character of the Coke Precursor in the Propane Direct Dehydrogenation on Pt Catalysts from a kMC Simulation. *ACS Catalysis* **2018**, *8*, 4694–4704.

(17) Lian, Z.; Si, C.; Jan, F.; Zhi, S.; Li, B. Coke Deposition on Pt-Based Catalysts in Propane Direct Dehydrogenation: Kinetics, Suppression, and Elimination. *ACS Catalysis* **2021**, *11*, 9279–9292.

(18) Nykänen, L.; Honkala, K. Selectivity in Propene Dehydrogenation on Pt and Pt $_3$ Sn Surfaces from First Principles. *ACS Catalysis* **2013**, *3*, 3026–3030.

(19) Yang, M.-L.; Zhu, Y.-A.; Zhou, X.-G.; Sui, Z.-J.; Chen, D. First-Principles Calculations of Propane Dehydrogenation over PtSn Catalysts. *ACS Catalysis* **2012**, *2*, 1247–1258.

(20) Mariscal, R.; Fierro, J. L.; Yori, J. C.; Parera, J. M.; Grau, J. M. Evolution of the properties of PtGe/Al2O3 reforming catalysts with Ge content. *Applied Catalysis A: General* **2007**, *327*, 123–131.

(21) Ballarini, A. D.; de Miguel, S.; Castro, A.; Scelza, O. n-decane dehydrogenation on bimetallic PtSn and PtGe catalysts prepared by dip-coating. *Catalysis in Industry* **2013**, *5*, 283–296.

(22) Hook, A.; Celik, F. E. Predicting Selectivity for Ethane Dehydrogenation and Coke Formation Pathways over Model Pt–M Surface Alloys with ab Initio and Scaling Methods. *The Journal of Physical Chemistry C* **2017**, *121*, 17882–17892.

(23) Borgna, A.; Garetto, T.; Apesteguia, C. Simultaneous deactivation by coke and sulfur of bimetallic Pt–Re(Ge, Sn)/Al2O3 catalysts for n-hexane reforming. *Applied Catalysis A: General* **2000**, *197*, 11–21.

(24) Kumar, M. S.; Chen, D.; Holmen, A.; Walmsley, J. C. Dehydrogenation of propane over Pt-SBA-15 and Pt-Sn-SBA-15: Effect of Sn on the dispersion of Pt and catalytic behavior. *Catalysis Today* **2009**, *142*, 17–23.

(25) Zandkarimi, B.; Alexandrova, A. N. Dynamics of Subnanometer Pt Clusters Can Break the Scaling Relationships in Catalysis. *Journal of Physical Chemistry Letters* **2019**, *10*, 460–467.

(26) Baxter, E. T.; Ha, M.-A.; Cass, A. C.; Alexandrova, A. N.; Anderson, S. L. Ethylene Dehydrogenation on Pt $_{4,7,8}$ Clusters on Al $_2$ O $_3$: Strong Cluster Size Dependence Linked to Preferred Catalyst Morphologies. *ACS Catalysis* **2017**, *7*, 3322–3335.

(27) Jo, Y.; Kim, T. W.; Oh, J.; Kim, D.; Suh, Y.-W. Mesoporous sulfur-decorated Pt–Al2O3 for dehydrogenation of perhydro benzyltoluenes: Activity-favorable adsorption of reaction species onto electron-deficient Pt atoms. *Journal of Catalysis* **2022**, *413*, 127–137.

(28) Poths, P.; Li, G.; Masubuchi, T.; Morgan, H. W. T.; Zhang, Z.; Alexandrova, A. N.; Anderson, S. L. Got Coke? Self-Limiting Poisoning Makes an Ultra Stable and Selective Sub-Nano Cluster Catalyst. *ACS Catalysis* **2023**, *13*, 1533–1544.

(29) Zhai, H.; Alexandrova, A. N. Local Fluxionality of Surface-Deposited Cluster Catalysts: The Case of Pt7 on Al2O3. *The Journal of Physical Chemistry Letters* **2018**, *9*, 1696–1702.

(30) Liu, G. X.; Poths, P.; Zhang, X. X.; Zhu, Z. G.; Marshall, M.; Blankenhorn, M.; Alexandrova, A. N.; Bowen, K. H. CO_2 Hydrogenation to Formate and Formic Acid

by Bimetallic Palladium-Copper Hydride Clusters. *Journal of the American Chemical Society* **2020**, *142*, 7930–7936.

(31) Halder, A.; Ha, M. A.; Zhai, H. C.; Yang, B.; Pellin, M. J.; Seifert, S.; Alexandrova, A. N.; Vajda, S. Oxidative Dehydrogenation of Cyclohexane by Cu vs Pd Clusters: Selectivity Control by Specific Cluster Dynamics. *Chemcatchem* **2020**, *12*, 1307–1315.

(32) Zhang, Z.; Zandkarimi, B.; Alexandrova, A. N. Ensembles of Metastable States Govern Heterogeneous Catalysis on Dynamic Interfaces. *Accounts of Chemical Research* **2020**, *53*, 447–458, Publisher: American Chemical Society.

(33) Lavroff, R. H.; Morgan, H. W. T.; Zhang, Z.; Poths, P.; Alexandrova, A. N. Ensemble representation of catalytic interfaces: soloists, orchestras, and everything in-between. *Chemical Science* **2022**, *13*, 8003–8016.

(34) Kresse, G.; Furthmuller, J. Efficient iterative schemes for ab initio total-energy calculations using a plane-wave basis set. *Physical Review B* **1996**, *54*, 11169–11186.

(35) Perdew, J. P.; Burke, K.; Ernzerhof, M. Generalized gradient approximation made simple. *Physical Review Letters* **1996**, *77*, 3865–3868.

(36) Blochl, P. E. Projector augmented wave method. *Physical Review B* **1994**, *50*, 17953–17979.

(37) Grimme, S.; Antony, J.; Ehrlich, S.; Krieg, H. A consistent and accurate iab initio/i parametrization of density functional dispersion correction (DFT-D) for the 94 elements H-Pu. *The Journal of Chemical Physics* **2010**, *132*, 154104.

(38) Sheppard, D.; Xiao, P. H.; Chemelewski, W.; Johnson, D. D.; Henkelman, G. A generalized solid-state nudged elastic band method. *Journal of Chemical Physics* **2012**, *136*, 8.

(39) Henkelman, G.; Uberuaga, B. P.; Jonsson, H. A climbing image nudged elastic band method for finding saddle points and minimum energy paths. *Journal of Chemical Physics* **2000**, *113*, 9901–9904.

(40) Bader, R. F. W. A quantum theory of molecular structure and its applications. *Chemical Reviews* **1991**, *91*, 893–928.

(41) Tang, W.; Sanville, E.; Henkelman, G. A grid-based Bader analysis algorithm without lattice bias. *Journal of Physics-Condensed Matter* **2009**, *21*.

(42) Zhai, H.; Alexandrova, A. N. Ensemble-Average Representation of Pt Clusters in Conditions of Catalysis Accessed through GPU Accelerated Deep Neural Network Fitting Global Optimization. *Journal of Chemical Theory and Computation* **2016**, *12*, 6213–6226.

(43) Maintz, S.; Deringer, V. L.; Tchougréeff, A. L.; Dronskowski, R. LOBSTER: A tool to extract chemical bonding from plane-wave based DFT. *Journal of Computational Chemistry* **2016**, *37*, 1030–1035.

(44) Dronskowski, R.; Blochl, P. E. Crystal orbital Hamiltonian populations (COHP) - Energy-resolved visualization of chemical bonding in solids based on density-functional calculations. *Journal of Physical Chemistry* **1993**, *97*, 8617–8624.

(45) Deringer, V. L.; Tchougreeff, A. L.; Dronskowski, R. Crystal Orbital Hamilton Population (COHP) Analysis As Projected from Plane-Wave Basis Sets. *Journal of Physical Chemistry A* **2011**, *115*, 5461–5466.

(46) te Velde, G.; Bickelhaupt, F. M.; Baerends, E. J.; Guerra, C. F.; Van Gisbergen, S. J. A.; Snijders, J. G.; Ziegler, T. Chemistry with ADF. *Journal of Computational Chemistry* **2001**, *22*, 931–967.

(47) Van Lenthe, E.; Baerends, E. J. Optimized Slater-type basis sets for the elements 1-118. *Journal of Computational Chemistry* **2003**, *24*, 1142–1156.

(48) Hauser, A. W.; Gomes, J.; Bajdich, M.; Head-Gordon, M.; Bell, A. T. Subnanometer-sized Pt/Sn alloy cluster catalysts for the dehydrogenation of linear alkanes. *Physical Chemistry Chemical Physics* **2013**, *15*, 20727.

(49) Hook, A.; Massa, J. D.; Celik, F. E. Effect of Tin Coverage on Selectivity for Ethane Dehydrogenation over Platinum–Tin Alloys. *The Journal of Physical Chemistry C* **2016**, *120*, 27307–27318.

(50) Wang, Z.; Chen, Y.; Mao, S.; Wu, K.; Zhang, K.; Li, Q.; Wang, Y. Chemical Insight into the Structure and Formation of Coke on PtSn Alloy during Propane Dehydrogenation. *Advanced Sustainable Systems* **2020**, *4*, 2000092.

(51) Furukawa, S.; Tamura, A.; Ozawa, K.; Komatsu, T. Catalytic properties of Pt-based intermetallic compounds in dehydrogenation of cyclohexane and n-butane. *Applied Catalysis A: General* **2014**, *469*, 300–305.

TOC Graphic